Height measurement of single nanoparticles based on evanescent field modulation

Takayuki Kurihara, Ryuichi Sugimoto,
Ryota Kudo, S. Takahashi* and K. Takamasu

Department of Precision Engineering,
School of Engineering,
The University of Tokyo,
Hongo 7-3-1, Bunkyo,
Tokyo, Japan
E-mail: kurihara@issp.u-tokyo.ac.jp
E-mail: sugimoto@nanolab.t.u-tokyo.ac.jp
E-mail: kudo@nanolab.t.u-tokyo.ac.jp
E-mail: takahashi@nanolab.t.u-tokyo.ac.jp
E-mail: takamasu@pe.t.u-tokyo.ac.jp
*Corresponding author

Abstract: We propose a novel height measurement method for single nanoparticles illuminated by an evanescent field in the total internal reflection microscopy scheme. The method utilises the scattered light intensity response to incident angle modulation. We introduced a physical model to derive a height measurement formula, and confirmed its validity through numerical simulations based on Maxwell's equation. We also verified the practical feasibility of the proposed method and confirmed that under an incident angle error of less than 0.1°, height measurement error of less than 10 nm could be achieved.

Keywords: nanoinspection; evanescent wave; particle measurement; near-field optics; total internal reflection microscopy; incident angle; Maxwell's equation; CMP process; microfluidic system; wafer inspection; nanomanufacturing.

Reference to this paper should be made as follows: Kurihara, T., Sugimoto, R., Kudo, R., Takahashi, S. and Takamasu, K. (2012) 'Height measurement of single nanoparticles based on evanescent field modulation', *Int. J. Nanomanufacturing*, Vol. 8, Nos. 5/6, pp.419–431.

Biographical notes: Takayuki Kurihara received his Bachelor's degree in the Precision Engineering from the University of Tokyo, Japan, in 2011. Currently, he belongs to the Master's course in the Department of Physics, School of Science, The University of Tokyo. His current research is the near-field optics and THz time domain spectroscopy of magnetic substances.

Ryuichi Sugimoto received his Bachelor's and Master's degrees in the Precision Engineering from the University of Tokyo, Japan in 2008 and 2010, respectively. He currently belongs to the Mitsui-Sumitomo Insurance Corporation.

Ryota Kudo received his Bachelor's and Master's degrees in the Precision Engineering from the University of Tokyo, Japan in 2007 and 2009, respectively. He currently belongs to the Doctoral course in the Department of

Copyright © 2012 Inderscience Enterprises Ltd.

Precision Engineering, School of Technology of the University of Tokyo. His current research is the semiconductor wafer inspection based on near field optics and image processing. He is a member of the JSPE.

Satoru Takahashi received his Bachelor's and Master's degrees in the Mechanical Engineering for Industrial Machinery and Systems from Osaka University, Japan in 1993 and 1995, respectively. He received his Doctor degree in Mechanical Engineering and Systems from Osaka University, Japan in 2002. He is currently an Associate Professor of the Department of Precision Engineering at the University of Tokyo, Japan. His research interests include the nano-in-process measurement and nano-scale-metrology based on the advanced optics using localised photon energy such as evanescent light, near-field light, and so on. He is a member of the ASPE, euspen, JSPE and JSME and an Associate Member of CIRP.

Kiyoshi Takamasu is a Professor of the Department of Precision Engineering in the University of Tokyo, Japan since 2001. He received his Bachelor's, Master's and Doctor degrees in Precision Engineering from the University of Tokyo, in 1977, 1979 and 1982, respectively. His research interests include precision measurement, coordinate measurement, nanometre measurement and calibration of precision instrument. He acted as a Visiting Researcher at Department of Engineering, University of Warwick, UK in 1990. He is a member of the euspen, JSPE, RSJ, IEEJ and SICE. He is the Chairman of the Technical Committee of Intelligent Measurement with Nanoscale in JSPE.

1 Introduction

Owing to the steady miniaturisation and growing complexity of micro and nanodevices, diverse new measurement techniques have emerged. As one of the basic configurations often encountered in nanoinspection, the height measurement of single nanoparticles located near a fine surface or interface is especially important in many nanomanufacturing applications.

For example, in studies on the mechanisms involved in the chemical mechanical polishing (CMP) process (Fang et al., 2000; Idei et al., 2011; Levert et al., 2000), the dynamical behaviour of colloidal particles near the wafer surface affects the quality of wafer planarisation; therefore, obtaining information on the height of each particle is required to clarify its role in this process (Idei et al., 2011; Lei et al., 2011; Zettner et al., 2003). As another example, in the study of three-dimensional fluid dynamics in the micro total analysis system (μTAS), the measurement of shear flow near the inner wall is important because this region dominates the velocity, resistance, and viscosity of flow. Fluid visualisation is usually realised by the particle image velocimetry (PIV) technique (Santiago et al., 1998; Meinhart et al., 1999), in which the movements of micro- or nanosized particles injected into the flow are measured by optical means. Here, the vertical position of particles near the wall is directly linked to the 3D-dynamics analysis of the shear flow (Li and Yoda, 2008; Meinhart et al., 2000; Yoda and Kazoe, 2011). In addition, in the silicon on insulator (SOI) wafer, the buried oxide (BOX) layer, a SiO_2 layer several hundred nanometers thick and embedded in the *Si* substrate contributes to high-speed device operation(Plößl and Kräuter, 2000). In terms of device quality and process control, the evaluation and/or inspection of information on the heights of

nanodefects in this layer is a topic of interest (Maszara, et al., 1988; Nakajima et al., 2005; Stoemenos et al., 1996; Kuwabara et al., 1999).

In these applications, an important issue is to measure the location of nanoparticles several tens of nanometers in diameter and positioned close (e.g., zero to several hundred nanometers) to the interface (Figure 1). Few methods are established for measurement of such configuration. One of the most effective is total internal refection (TIR) microcopy, a near-field optics technique that uses an evanescent field as illumination.

Figure 1 Concept of nanoparticle height measurement

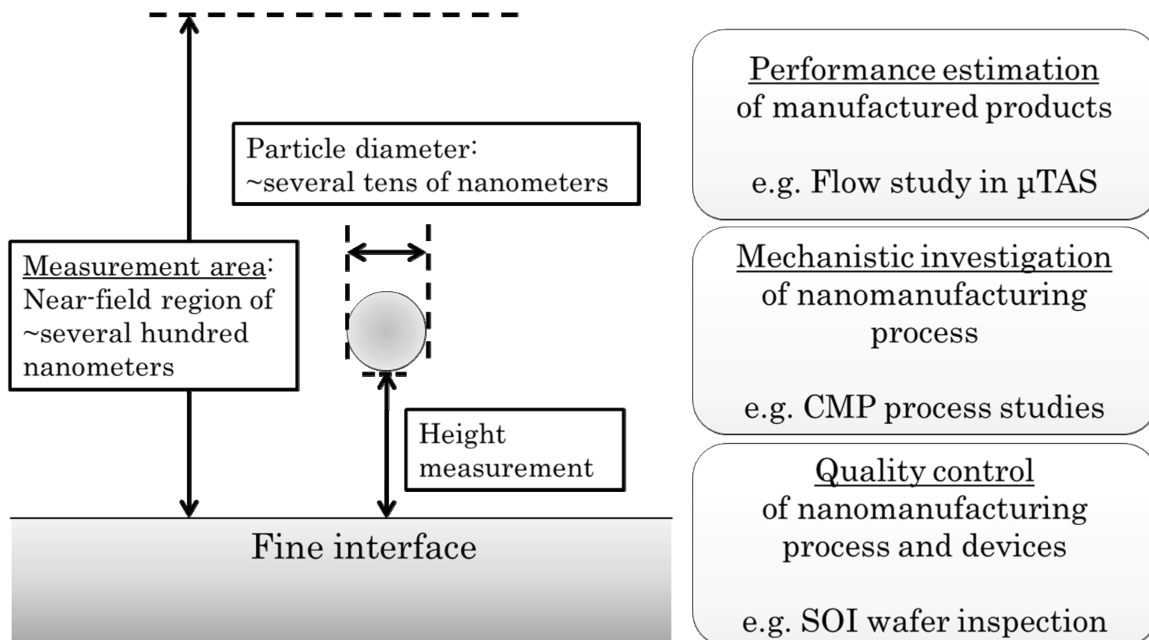

An evanescent wave, which is produced as light undergoes total reflection at a refractive index interface, is a vertically localised electromagnetic energy near the interface. The use of this form of illumination in microscopic observations is advantageous compared with far-field light in terms of the signal to noise (S/N) ratio, in near-interface measurements (Axelrod, 1989; Gankin et al., 2011; Kanda et al., 2007; Zettner, 2001). For example, in a study of CMP slurry dynamics, Idei et al. (2011) used this technique to successfully measure phenomena related to the adhesion of SiO_2 particles to the wafer surface during the polishing process. In addition, in a study of SOI wafer inspection, Nakajima applied the TIR technique with scanning near-field optical microscopy (SNOM) to inspect nanometre-sized defects in the BOX layer (Nakajima et al., 2005).

In some recent studies of near-interface imaging, TIR microscopy has often been extended to nanoparticles height measurement to take advantage of its high S/N ratio. The typical principles of height measurement are as follows. The characteristic spatial distribution of an evanescent wave along the vertical direction strongly affects the intensity of light scattered from nanoparticles near the interface. Therefore, the scattered light conveys important information on the height of particles. In conventional applications, the height of a nanoparticle (or defect) is measured from the intensity of light scattered from the object by using information on the exponential decay characteristics of the evanescent wave (Kanda et al., 2007).

However, this conventional technique of particle height measurement with an evanescent wave has the problem that the absolute height cannot be obtained from a single measurement; it requires additional measurements of the intensity of light scattered from particles known to be attached to the TIR interface for calibration or zero-offset. As the application of particle height measurement with an evanescent wave becomes widespread, a simpler method that does not require such a procedure to obtain the absolute height of individual particles will become necessary.

In this paper, we propose a novel method for measuring the absolute height of nanoparticles located near the TIR interface by using the scattered light intensity response to a change in the evanescent field distribution. This method is based on the observation that the intensity of light scattered from a nanoparticle strongly depends on its height from the TIR interface and also on the penetration depth of the evanescent field. As the latter can be controlled by a change in the incident angle, we can calculate the actual height of nanoparticle by tracing the scattered light intensity response to such a change. In this paper, a method using two incident angles, which is the simplest case, is studied as the first step of verification.

The rest of this paper is organised as follows. In Section 2, we introduce the nanoparticle scattering model, and describe the principle underlying the height measurement method based on two incident angles. In Sections 3 and 4, we carry out a numerical simulation based on Maxwell's equation to show that the proposed method is valid for nanoparticles with heights in the range of several hundred nanometers from the TIR surface. In Section 5, in order to verify the practical feasibility of the method, we discuss the effect of incident angle error, which can be thought of as the dominant error source upon measurement.

2 Principles of height measurement

Light undergoes total internal reflection at the refractive index interface when it passes from the side with the higher refractive index (n_1) medium to that with the lower one (n_2), at an incident angle exceeding the critical angle $\theta_c = \sin^{-1}(n_2/n_1)$. Evanescent light, i.e., electromagnetic energy localised in order of the wavelength of the incident light, is produced in the side with the lower refractive index medium (Born, 1988).

Generally, the electric field component of an evanescent wave has the following form:

$$E(\theta, z) = E(\theta, 0) \cdot \exp\left(\frac{-z}{2d(\theta)}\right) \tag{1}$$

where z is the height measured from the TIR interface, θ is the incident angle, $E(\theta, 0)$ is the electric field vector at the interface, and $d(\theta)$ is the penetration depth, which characterises the spatial distribution of evanescent light. For simplicity, we assume that the direction of $E(\theta, 0)$ is parallel to the TIR interface, i.e., that the incident light is S-polarised. The penetration depth depends on the incident angle and is represented by the following equation:

$$d(\theta) = \frac{\lambda_0}{4\pi\sqrt{n_1^2 \sin^2\theta - n_2^2}} \tag{2}$$

where λ_0 is the wavelength of the incident light in vacuum.

Here, we introduce a dielectric nanoparticle located near the TIR interface and illuminated by evanescent light [Figure 2(a)]. Given the exponential decay of the evanescent field, the total intensity of scattered light from the particle is also expected to have the exponential form:

$$S(\theta, z) = S(\theta, 0) \cdot \exp\left(\frac{-z}{d(\theta)}\right) \quad (3)$$

where $S(\theta,0)$ is the intensity of light scattered from the particle when it is closely attached to the TIR interface.

Figure 2 Schematic of the configuration (a), and scattered light intensity response to a change in the incident angle ((b) and (c))

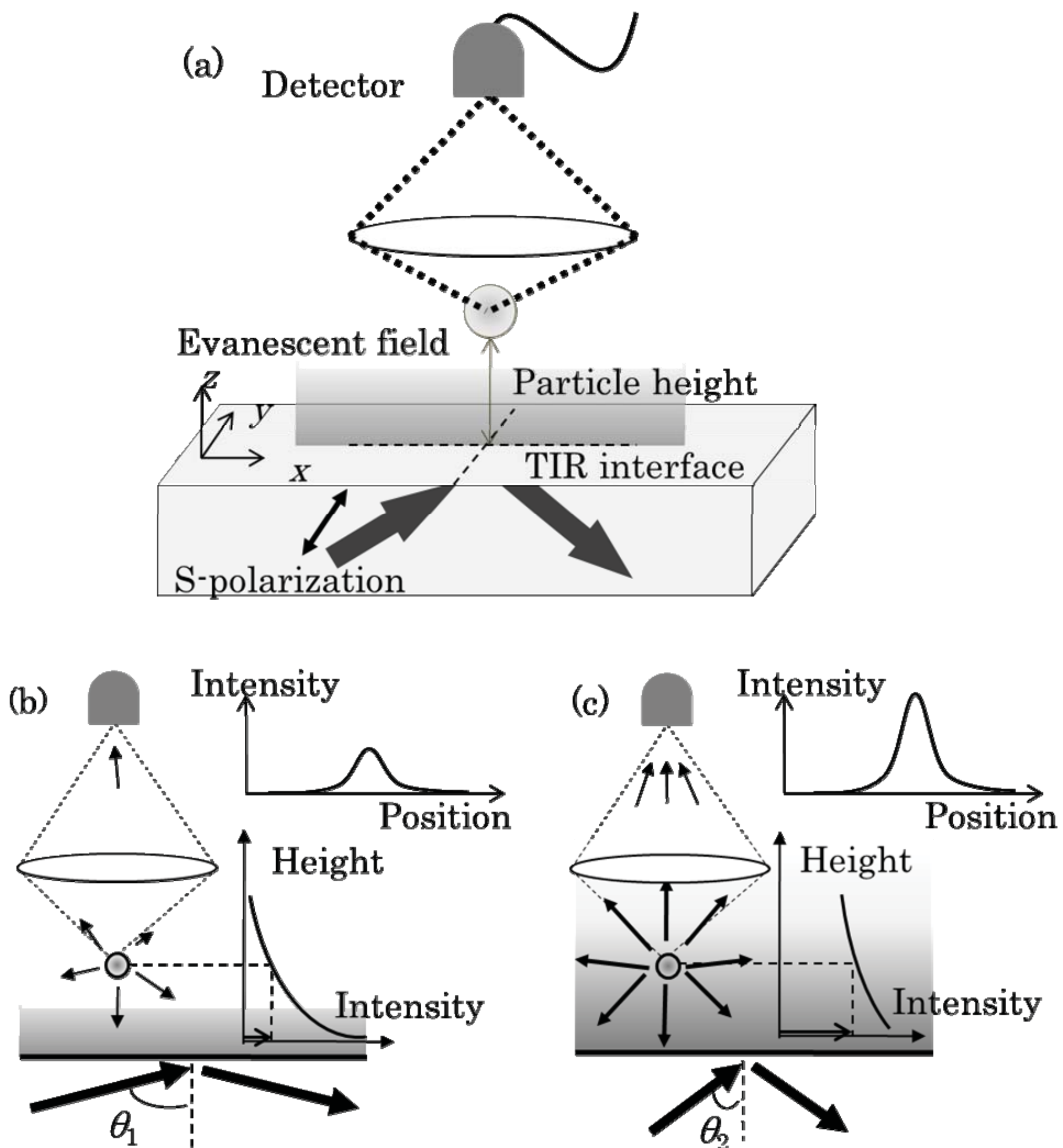

In order to further express the scattered intensity observed on the image plane, we have to take into account the effects of imaging optics and the existence of the refractive index interface. Under approximations we describe later, they can be expressed in the form of functions multiplied to equation (3) and given as follows:

$$M = S(\theta, z) = S(\theta, 0) \cdot \exp\left(\frac{-z}{d(\theta)}\right) \cdot \mathrm{psf}(z) \cdot C(z) \quad (4)$$

where psf(z) is the point spread function along the z-axis of the imaging optics, and $C(z)$ is the effect of interference between radiation from the particle and its mirror image induced in the higher refractive index medium. As expected, we cannot calculate the particle height from the observed signal M alone, because generally the forms of $C(z)$, psf(z), and $S(\theta, 0)$ are unknown. However, assuming that the right-hand side of equation (4) involves θ only in the exponential term and $S(\theta, 0)$ term, we can regard θ as a parameter and calculate z from M measured at multiple incident angles.

Given that the penetration depth is a function of the incident angle, when the particle is illuminated by evanescent waves of two different incident angles [Figures 2(b), (c)], the corresponding scattered intensity to be observed (M_1 and M_2) can be expressed as follows:

$$M_1 \equiv S(\theta_1, z) = S(\theta_1, 0) \cdot \exp\left(\frac{-z}{d(\theta_1)}\right) \cdot \mathrm{psf}(z) \cdot C(z) \quad (5)$$

$$M_2 \equiv S(\theta_2, z) = S(\theta_2, 0) \cdot \exp\left(\frac{-z}{d(\theta_2)}\right) \cdot \mathrm{psf}(z) \cdot C(z) \quad (6)$$

By dividing equation (5) by equation (6), we can derive the following expression for z without considering the unknown terms:

$$z_{cal} = \frac{1}{\dfrac{1}{d(\theta_2)} - \dfrac{1}{d(\theta_1)}} \log\left[\frac{M_1}{M_2} \frac{S(\theta_2, 0)}{S(\theta_1, 0)}\right] \quad (7)$$

Here, the form of $S(\theta_1, 0)/S(\theta_2, 0)$ must be derived by theoretical means. To do so, we assume several realistic approximations as follows:

1 The electromagnetic filed is static inside the particle.

2 The original electromagnetic distribution of the evanescent field is unchanged by the existence of the nanoparticle.

3 The electric polarisation inside the particle is proportional to the original electric field distribution of the evanescent field.

These approximations are expected to hold when the disturbance of the evanescent wave by the particle is small, i.e., the scattering by the particle is sufficiently small. From these approximations, we can derive the following formula for $S(\theta, 0)$ for a spherical nanoparticle of diameter a [equation (8)]. Here, the electric polarisation inside the particle is integrated over the volume (Figure 3):

$$S(\theta,0) \propto \left\{ \iiint_{particle} \varepsilon E_0(\theta, z')dV \right\}^2$$

$$= \left\{ \int_0^{\alpha} dz' \Delta V(z') \cdot \varepsilon E_0(z') \right\}^2 \qquad (\varepsilon : \text{dielectric constant})$$

$$= \left\{ \int_0^{\alpha} dz' \pi \left[\left(\frac{\alpha}{2}\right)^2 - \left(\frac{\alpha}{2} - z'\right)^2 \right] \cdot \varepsilon E_0 \cos\theta \cdot e^{\frac{-z'}{2d(\theta)}} \right\} \tag{8}$$

$$= S_0 \cdot \cos^2\theta \left\{ ad(\theta)^2 - 4d(\theta)^3 + \left[4d(\theta)^3 + ad(\theta)^2 \right] \exp\left(\frac{-a}{2d(\theta)} \right) \right\}^2$$

Figure 3 Configuration for polarisation calculation (see online version for colours)

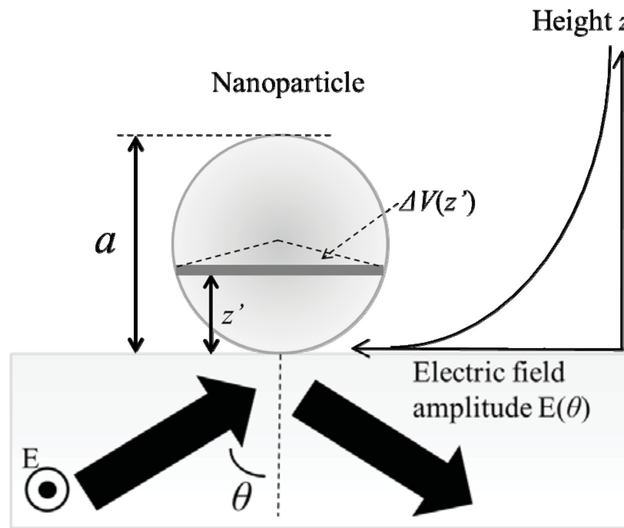

As can be seen from the form of equation (4), the measured particle height is independent of the scattered light detection efficiency of the individual experimental setup; in practice, this is one of the advantages of the method. For example, changing the numerical aperture (NA) of the imaging optics changes only the term psf(z), which is cancelled out in equation (7). Therefore, the calculated height z_{cal} remains unchanged.

3 Verification of proposed method by FDTD simulation

In order to verify the proposed method, a numerical simulation based on Maxwell's equation was carried out. Here, the FDTD (finite-distance Time-domain) method (Yee, 1966) is used for the calculations. A schematic of the setup and the parameters of the simulation are shown in Figure 4 and Table 1, respectively. A dielectric particle with a diameter of 50 nm and a refractive index n_3 of 1.59 is located in a medium with a refractive index n_2 of 1 and is illuminated by evanescent field. Here, the particle height Z is varied from 0 to 250 nm in 50 nm steps. For each particle height two incident angles were used for generating the evanescent field and at each angle the intensity of light

scattered by the particle is recorded. Here, the intensity of light scattered by the particle is defined as the time average of total electromagnetic energy absorbed by the perfectly matched layer (PML) boundary 60µm above the TIR surface. The particle height was calculated with the proposed method by using these data.

Figure 4 Schematic of FDTD simulation setup

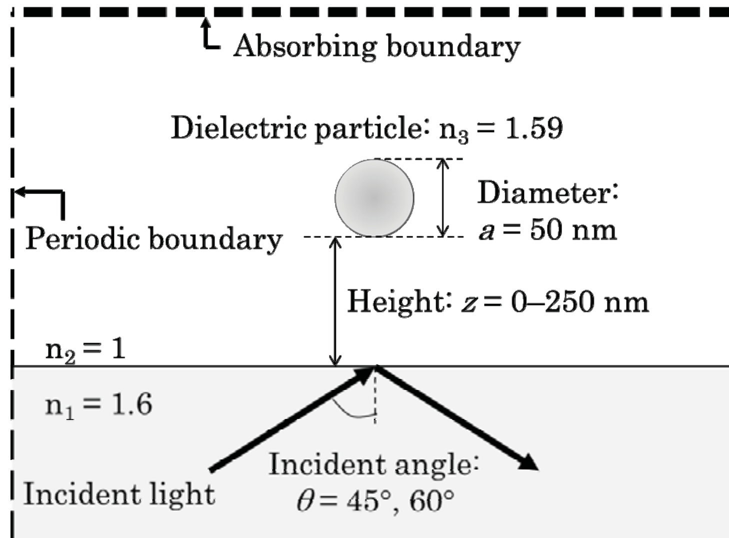

Table 1 Parameter values

Item	*Value*
Wavelength: l	532 nm
Particle height: z	0–250 nm (50 nm step)
Particle diameter: a	50 nm
Lower refractive index: n_1	1.0
Higher refractive index: n_2	1.6
Refractive index of particle: n_3	1.59
Incident angle: θ	45°, 60°
Critical angle: θ_c	38.8°

Figure 5 Electric field distribution of light scattered from the nanoparticle obtained from the FDTD simulation. The particle is located (a) 50 nm or (b) 100 nm above TIR interface and illuminated by an evanescent light with an incident angle θ of 45°

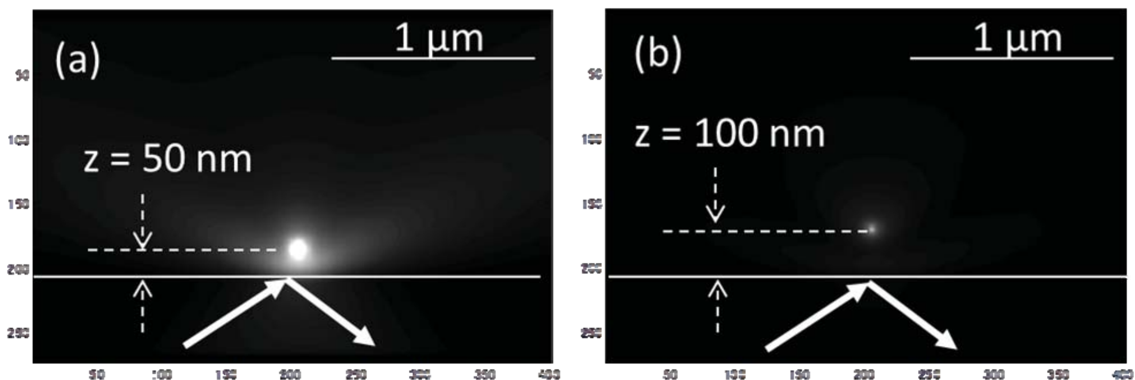

4 Simulation result

The particle height calculated by the proposed method is shown in Figure 6. The horizontal and vertical axes of the graph correspond to the setup height and calculated particle height, respectively. That the calculated height is in good agreement with the setup height supports the validity of the proposed method. From this result we confirmed that the height of a particle 50 nm in diameter at a distance of 0–200 nm from the interface can be measured with an error of around 20 nm. We can also conclude that within this setup the form of $S(\theta, 0)$ given by equation (8), which is based on the three approximations in Section 2, is valid.

Figure 6 Height calculated from the FDTD simulation (vertical axis) vs. setup height (horizontal axis)

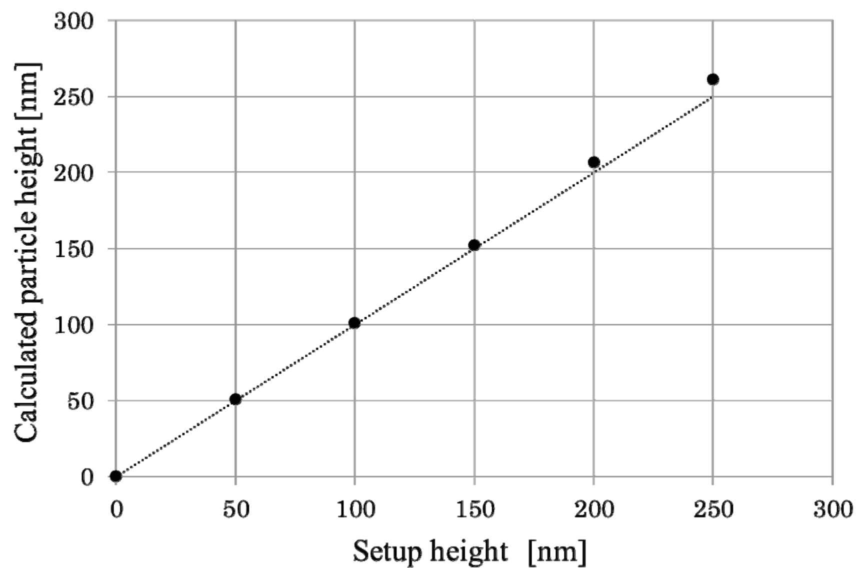

5 Error evaluation for practical application

In order to verify the practical feasibility of proposed method, we calculated the error quantity induced by the errors in the setting parameters. Considering the characteristics of the proposed method, assuming that the form of $S(\theta, 0)$ is valid (as was confirmed from the previous simulation), one of the dominant error sources to the measurement in practical conditions is the error of setting the incident angles. In order to understand this effect, we calculated the height of a particle positioned at a given height, by using an incident angle containingan error of ~±0.1°. Here, as a typical value, the setup height was chosen to be z = 100 nm. Other parameters, e.g., the refractive indices of the media or the critical angle, are the same as those used in Section 3. Here, $S(\theta, z)$ was calculated from equation (3) by using the given incident angles without error, and the particle height z was calculated from equation (7) by using error-embedded incident angles.

Figure 7 shows the calculated result for (θ_1, θ_2) = (45°, 60°). The *X*- and *Y*- axis correspond to the amounts of incident angle error embedded inθ_1 and θ_2 ($\Delta\theta$ of 0° to ±0.1°), respectively, and the Z-axis represents the height calculated from equation (7)

using these error-embedded incident angles. The calculation error is explicitly equal to zero for the point $\Delta\theta_1 = \Delta\theta_2 = 0$. The calculation error increases for the region of $\Delta\theta_1 \cdot \Delta\theta_2 < 0$ region, i.e., when the two incident angles have errors in the opposite direction. In contrast, the calculation error is comparatively small if $\Delta\theta_1 - \Delta\theta_2$, i.e., when both incident angles shift in the same direction. Practically, this means that even if measuring the absolute values of the incident angles is difficult, the angle-induced error is comparatively small as long as the difference of two angles can be precisely measured. In other words, the 'DC-bias' embedded in the incident angles does not have much effect upon the height-error. This is one of the advantages of the method.

Figure 7 Height calculated by using error-embedded incident angles (see online version for colours)

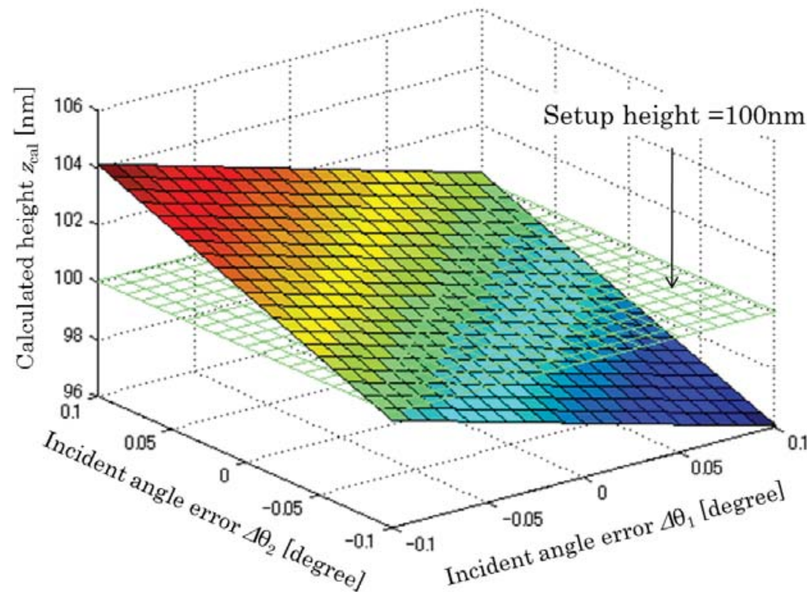

Notes: Centre angles are $(\theta_1, \theta_2) = (45°, 60°)$. The difference between the maximum and minimum is 8.1 nm.

Next, we calculated the error quantity induced by an angle error of ±0.1° for various sets of incident angles (θ_1, θ_2). Here, the error quantity at each set of angles, which was defined as the difference between the maximum and minimum value of the calculation result as in Figure 7, was plotted for each angle set (Figure 8).

The calculation error is comparatively small for sets of incident angles that are far apart from one another. In contrast, the calculation error diverges to infinity as the two angles approach. This is because the denominator term of equation (7) approaches zero for $\theta_1 - \theta_2$. In practice, the use of two incident angles as far apart from one another as possible, one of them being slightly above the critical angle, is beneficial in the sense that it decreases the angle-induced measurement error.

From these calculations, we can find the optimal set of incident angles when alignment or measurement errors are involved. For example, Figure 8 shows that in order to achieve height error of <10 nm under the angle error of ±0.1°, then (θ_1, θ_2)–(41°, >63°) should be chosen. In the above case, for example, an error of $\Delta z = 5.74$ nm is achieved at $(\theta_1, \theta_2) = (41°, 68°)$.

In summary, for a given amount of angle error, the set of incident angles should be properly chosen in order to minimise the calculation error. Typically, the two angles should be chosen to be as far apart from one another as possible, with one of them being slightly above the critical angle. However, in practice, choosing an incident angle too close to the critical angle can cause instability in height calculation because the scattered intensity response is abrupt near this angle. Therefore, numerical estimations similar to those performed here are required in order to find the set of incident angles that gives the optimal height error.

Figure 8 Effect of angle error upon measurement. A minimum error of 5.7 nm is obtained at $(\theta_1, \theta_2) = (68°, 41°)$, whereas the error diverges around $\theta_1 - \theta_2$ (see online version for colours)

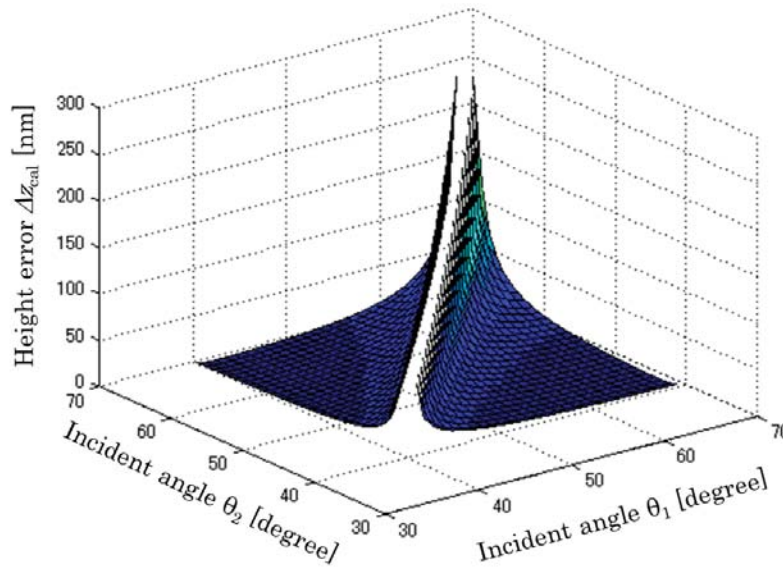

6 Conclusions

We proposed a technique to measure the height of single nanoparticles by using evanescent field modulation. This technique can be applied to various nanomanufacturing and inspection applications. We confirmed the validity of the proposed method and its basic assumptions through a numerical simulation based on Maxwell's equation. We showed that the proposed method can calculate the height of a 50 nm diameter particle with an accuracy of ~20 nm within the height region of 0 – 250 nm. Finally, we calculated the effect of angle error upon measurement. The result showed that with an angle error of <0.1°, two incident angles properly chosen can give a measurement error of below 10 nm.

In future studies, we intend to provide more precise range estimates for parameters such as the size and shape of the particle, refractive index difference between the particle and surrounding medium, and the polarisation direction of incident light. We should also note that although only two incident angles were considered in this paper, similar methods that use more angles can be applied for enhanced feasibility. In addition, we will evaluate the throughput and/or possible measurement time scale of the proposed method in future studies.

Acknowledgements

This work was supported by JSPS under a Grant-in-Aid for ScientificResearch (A) and a Grant-in-Aid for Challenging Exploratory Research.

References

Axelrod, D. (1989) 'Total internal reflection fluorescence microscopy', *Methods in Cell Biology*, Vol. 30, Issue C, p.245.

Born, M. and Wolf, E. (1980) *Principle of Optics*, 6th ed., pp.418–424, Pergamon Press, New York.

Fang, S.J., Garza, S., Guo, H., Smith, T.H., Shin, G.B., Campbell, J.E. and Hartsell, M.L. (2000) 'Optimization of the chemical mechanical polishing process for premetal dielectrics', *Journal of the Electrochemical Society*, Vol. 147, No. 2, pp.682–686.

Gankin, M., Popescu, S.A., Apter, B., Mirchin, N., Lapsker, I. and Peled, A. (2011) 'Differential evanescent light intensity imaging of nanothin films: simulation of the scattered field', *Physica Status Solidi (c)*, Vol. 8, No. 9, pp.2957–2960.

Idei, Y., Kimura, K., Suzuki, K., Khajornrungruang, P. and Johyama, J. (2011) 'Observation of fine particles motion during CMP process by evanescent field', *Proceedings of the 17th Kanto Branch Regular Meeting of the Japan Society of Mechanical Engineers*, Vol. 3, No. 17, pp.571–572.

Kanda, K., et al. (2007) 'Measurement of particle distribution in microchannel flow using a 3D-TIRFM technique', *Journal of Visualization*, Vol. 10, No. 2, pp.207–216.

Kuwabara, S., Minami, K., Yatsugake, Y. and Kato, Y. (1999) 'Detection of particles on quarter μm thick or thinner SOI wafers', *Journal of Applied Physics*, Vol. 38, No. 4B, pp.2506–2509.

Lei, J., Guo, D., Luo, J. and Pan, G. (2011) 'Probing particle movement in CMP with fluorescence technique', *Journal of the Electrochemical Society*, Vol. 158, No. 6, pp.H681–H685.

Levert, J.A., Dayluk, S. and Tichy, J. (2000) 'Mechanism for subambient interfacial pressures while polishing with liquids', *Journal of Tribology – Transactions of the ASME*, Vol. 122, No. 2, pp.450–457.

Li, H.F. and Yoda, M. (2008) 'Multilayer nano-particle image velocimetry (MnPIV) in microscale Poiseuille flows', *Measurement Science and Technology*, Vol. 19, No. 075402, 9pp.

Maszara, W.P., et al. (1988) 'Bonding of silicon wafers for silicon-on-insulator', *Journal of Applied Physics*, Vol. 64, No. 10, p.4943.

Meinhart, C.D., Werely, S.T. and Gray, M.H.B. (2000) 'Volume illumination for two-dimensional particle image velocimetry', *Measurement Science and Technology*, Vol. 11, No. 6, pp.809–814.

Meinhart, C.D., Werely, S.T. and Santiago, J.G. (1999) 'PIV measurements of a microchannel flow', *Experiments in Fluids*, Vol. 27, No. 5, pp.414–419.

Nakajima, R., Miyoshi, T. and Takaya, Y., (2005) 'Novel nano-defect measurement method of SOI wafer using evanescent light', *Proceedings of.the SPIE Optics East 2005 Symposium*, 6013, 60130N

Plößl, A. and Kräuter, G. (2000) 'Silicon-on-insulator: materials aspects and applications', *Solid-State Electron*ics, Vol. 44, No. 5, pp.775–782.

Santiago, J.G., Werely, S.T., Meinhart, C.D., Beebe, D.J. and Adrian, R.J. (1998) 'A particle image velocimetry system for microfluidics', *Experiments in Fluids*, Vol. 25, No. 4, pp.316–319.

Stoemenos, J. (1996) 'Structural defects in SIMOX', *Nuclear Instruments and Methods B*, Vol. 112, Nos. 1–4, pp.206–213.

Yee, K.S. (1966) 'Numerical solution of initial boundary value problems involving Maxwell's equations in isotropic media', *IEEE Transactions on Antennas Propagation*, Vol. 14, No. 3, pp.302–307.

Yoda, M. and Kazoe, Y. (2011) 'Dynamics of suspended colloidal particles near a wall: implications for interfacial particle velocimetry', *Physics of Fluids*, Vol. 23, No. 11, p.111301.

Zettner, C.M. (2001) *Visualization of Particle Dynamics at Various Spatial Scales*, PhD thesis, School of Mechanical Engineering, Georgia Institute of Technology, Atlanta, United States of America.

Zettner, C.M. and Yoda, M. (2003) 'Particle velocimetry measurements in a near-wall flow using evanescent wave illumination', *Experiments in Fluids*, Vol. 34, No. 1, pp.115–121.